Pergamon

Journal of Structural Geology, Vol. 20, No. 11, pp. 1549 to 1568, 1998

PII: S0191-8141(98)00044-3

0191-8141/98 $ - see front matter

c-Axis fabrics and microstructures in quartz schist from the Sambagawa metamorphic belt, central Shikoku, Japan

MASAHIKO TAGAMI and TORU TAKESHITA*

Department of Earth and Planetary Systems Science, Faculty of Science, Hiroshima University, Higashi-Hiroshima 739-8536, Japan. E-mail: toru@letitbe.geol.sci.hiroshima-u.ac.jp

(*Received* 3 *January* 1997; *accepted in revised form* 30 *April* 1998)

Abstract—An integrated study on *c*-axis fabric and microstructure of plastically deformed and dynamically recrystallized quartz in quartz schist from the Sambagawa metamorphic belt in central Shikoku, Japan has revealed a correlation between *c*-axis fabrics and three-dimensional grain shape. Recrystallized quartz grains with prolate ($k > 1$), oblate ($0.2 < k < 1$) and uniaxially oblate ($k < 0.2$) shapes exhibit *c*-axis fabric patterns of cleft girdles around the principal finite elongation direction (X), type I crossed girdles, and small circle girdles around the principal finite shortening direction (Z), respectively. Fabric intensity calculated from the eigenvalues of orientation tensors of the *c*-axis fabrics increases with increasing magnitude of the *apparent* finite strain inferred from the shape of recrystallized quartz grains. These results indicate that the development of recrystallized grain shape as well as *c*-axis fabrics is primarily controlled by finite strain during progressive deformation. However, the finite strain estimated from three-dimensional grain shape is systematically deviated toward the flattening field compared to that estimated from the *c*-axis fabrics. We investigated several possible causes for the discrepancy, and propose that a scenario of coupled deformation and dynamic recrystallization in the quartz schist is responsible for the formation of these microstructures.

INTRODUCTION

Intracrystalline slip systems and lattice preferred orientation (LPO) development in quartz single crystals and aggregates during deformation have been experimentally analyzed by many authors (e.g. Heard and Carter, 1968; Baëta and Ashbee, 1969a,b; Green *et al.*, 1970; Tullis *et al.*, 1973; Tullis, 1977). Many theoretical studies have also been carried out on these subjects based on various polycrystal plasticity models (e.g. Etchecopar, 1977; Lister *et al.*, 1978; Etchecopar and Vasseur, 1987; Wenk *et al.*, 1989). These experimental and theoretical results have been applied to LPOs in natural quartzite in order to infer aspects of deformation kinematics such as the strain path and strain intensity (see a review by Price, 1985), and temperature conditions during deformation (e.g. Lister and Dornsiepen, 1982).

c-Axis fabrics in natural quartzites which suffered coaxial progressive deformation under greenschist conditions have been reported by many authors (e.g. Law *et al.*, 1984, 1986; Schmid and Casey, 1986), and the relationship between the *c*-axis fabric patterns and finite strain mode estimated from the deformed shape of detrital grains has been analyzed (e.g. Marjoribanks, 1976; Bouchez, 1977; Miller and Christie, 1981; Law, 1986). These analyses have shown that when the strain indicators exhibit constrictive, plane strain and flattening strain mode, the *c*-axis fabrics show cleft girdles, type I crossed girdles and small circle girdles, respectively. Furthermore, these studies have indicated that *c*-axis fabric intensity increases with increasing finite strain. It has been therefore concluded that the pattern and intensity of the quartz *c*-axis fabrics are primarily controlled by finite strain (kinematic control).

In fully recrystallized quartz aggregates such as quartz schist, there is no reliable finite strain indicator. There have been few analyses of the relationship between the LPO and grain shape in fully recrystallized quartz based on finite strain. In this study, we have analyzed both the *c*-axis fabrics and recrystallized quartz grain shape fabrics in quartz schist samples which were collected from the Sambagawa metamorphic belt, central Shikoku, Japan. Recrystallized quartz grain shape fabrics, both the mean grain aspect ratio and R–Φ ratios, have been analyzed to infer the *apparent* strain ratios (i.e. aspect ratios of the strain ellipse) in two orthogonal thin sections. These strain ratios are *apparent* because recrystallized grains change their shape through both deformation and recrystallization. Subsequently, both the k-values and strain magnitude $\bar{\varepsilon}_s$ for the grain shape fabrics have been calculated from the *apparent* strain ratios in each thin section. Throughout this study, we used the terms 'prolate' and 'oblate' when we refer to the shapes of recrystallized quartz grains, while the terms 'constrictive' and 'flattening' were used to indicate the finite strain. The k-values and strain magnitude $\bar{\varepsilon}_s$ have been compared with *c*-axis fabric patterns and intensity, respectively, and their relationships have been analyzed.

*To whom all correspondence should be addressed.

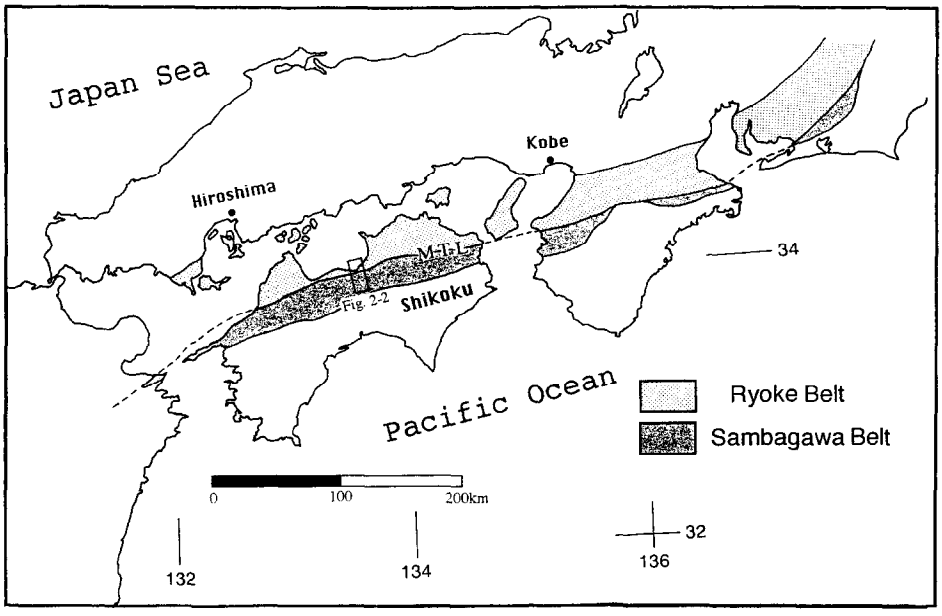

Fig. 1. Index map of the Sambagawa and Ryoke metamorphic belts in southwestern Japan. MTL: Median Tectonic Line. A box in central Shikoku marks the region of Fig. 2.

GEOLOGICAL SETTING

The Sambagawa (or Sanbagawa) belt is a high P/T type metamorphic belt in southwestern Japan (*ca* 800 km long). It is juxtaposed in the north against the Ryoke low P/T type metamorphic belt, bounded by the Median Tectonic Line (MTL) (Fig. 1). These two belts are regarded as a so-called *paired metamorphic belt* (Miyashiro, 1961). The Sambagawa metamorphic belt originated from accretionary complexes which formed from late Jurassic to early Cretaceous (Iwasaki *et al.*, 1984). On the basis of metamorphic mineral equilibrium, the estimated peak metamorphic conditions of the Sambagawa metamorphic rocks in central Shikoku reached about 600°C and 10 kbar in the highest grade part (e.g. Banno and Sakai, 1989; Enami *et al.*, 1994). K–Ar and $^{40}Ar/^{39}Ar$ mineral radiometric ages of the Sambagawa metamorphic rocks in central Shikoku vary between 94 and 70 Ma (e.g. Itaya and Takasugi, 1988; Isozaki and Itaya, 1990), suggesting that the exhumation started in late Cretaceous.

The deformation structures in the Sambagawa metamorphic belt have been divided into the following three major deformation phases (e.g. Hara *et al.*, 1977; Faure, 1983). D_1 is characterized by the formation of dominant bedding schistosity (S_1) and E–W-trending horizontal stretching mineral lineation (L_1), which is nearly parallel to the trend of the belt. Intrafolial, sheath and curvilinear folds (F_1) also characterize the D_1 phase, the axial surfaces of which are parallel to S_1. Although this phase was once regarded as synchronous with the peak metamorphism (e.g. Faure, 1983; Banno and Sakai, 1989), it has since been realized that the deformation mainly took place under retrograde conditions during the exhumation (e.g. Hara *et al.*, 1992; Wallis *et al.*, 1992). D_2 phase (Ozu–Nagahama phase: Hara *et al.*, 1977) is recognized by south-verging, overturned folds (F_2) on several scales, and thrust faults and associated axial plane cleavages (microlithons). D_3 (Hijikawa Phase: Hara *et al.*, 1977) structures are recognized in outcrop as open upright folds with E–W-trending horizontal axes (F_3). These outcrop scale minor folds are believed to be parasitic (or drag) folds of map-scale sinistral en échelon D_3 folds with a wavelength of several km. Figure 2 shows the axial traces of the large scale D_3 folds.

In the studied area, in the central part of the Asemi–gawa river region, the Sambagawa metamorphic rocks consist of pelitic schist, basic schist and quartz schist, with lesser amounts of psammitic schist. Tectonic blocks of ultramafic rocks are sparsely distributed in the area. The schistosity is parallel to the bedding surface (i.e. bedding schistosity, S_1) in this region, and strikes WNW–ESE to E–W and dips 30–50° northward, exhibiting a homoclinal structure. A mineral stretching lineation (L_1) trends WNW–ESE and plunges horizontally.

A metamorphic zonation has been established in the Asemi–gawa river area based on mineral assemblages in the basic and pelitic schists (e.g. Banno and Sakai, 1989; Higashino, 1990; Hara *et al.*, 1990a). The metamorphic zone boundaries are approximately parallel to the bedding schistosity (S_1). The metamorphic zones are stacked in the structural ascending order: chlorite, garnet, albite–biotite, oligoclase–biotite, albite–biotite and garnet zones (Fig. 2). Therefore, the highest-grade oligoclase–biotite zone is located at the middle structural level. This peculiar geologic structure has been attributed to the formation of either a large scale

recumbent fold (e.g. Banno and Sakai, 1989) or nappes (e.g. Hara *et al.*, 1990b) after the peak metamorphism.

GENERAL DESCRIPTION OF THE SAMBAGAWA QUARTZ SCHIST

Quartz schist occurs as relatively thin layers (between several cm and 10 m thick) within thick pelitic or basic schist layers. The protolith of the quartz schist has been interpreted to be radiolarian chert, because relatively low-grade rocks include abundant radiolarian fossils (e.g. Toriumi, 1982; Shimizu, 1988). Studied samples were collected from the upper chlorite zone to the lower garnet zone (Fig. 3) and are composed mostly of recrystallized quartz grains (>90%) and lesser amount of accessory minerals such as actinolite, muscovite, chlorite, garnet, albite, epidote and hematite. The quartz schist grades structurally upwards (or downwards) into either pelitic or basic schist with increasing volume fractions of muscovite, or epidote and actinolite, respectively.

Parallel arrangement of flaky minerals such as chlorite and muscovite defines S_1 in the quartz schist. L_1 is defined by a shape preferred orientation of quartz, piedmontite, or spindle-shaped plagioclase porphyroblasts. S_1 is often folded by later phase deformations (F_2 and/or F_3). We collected samples with only a pla-

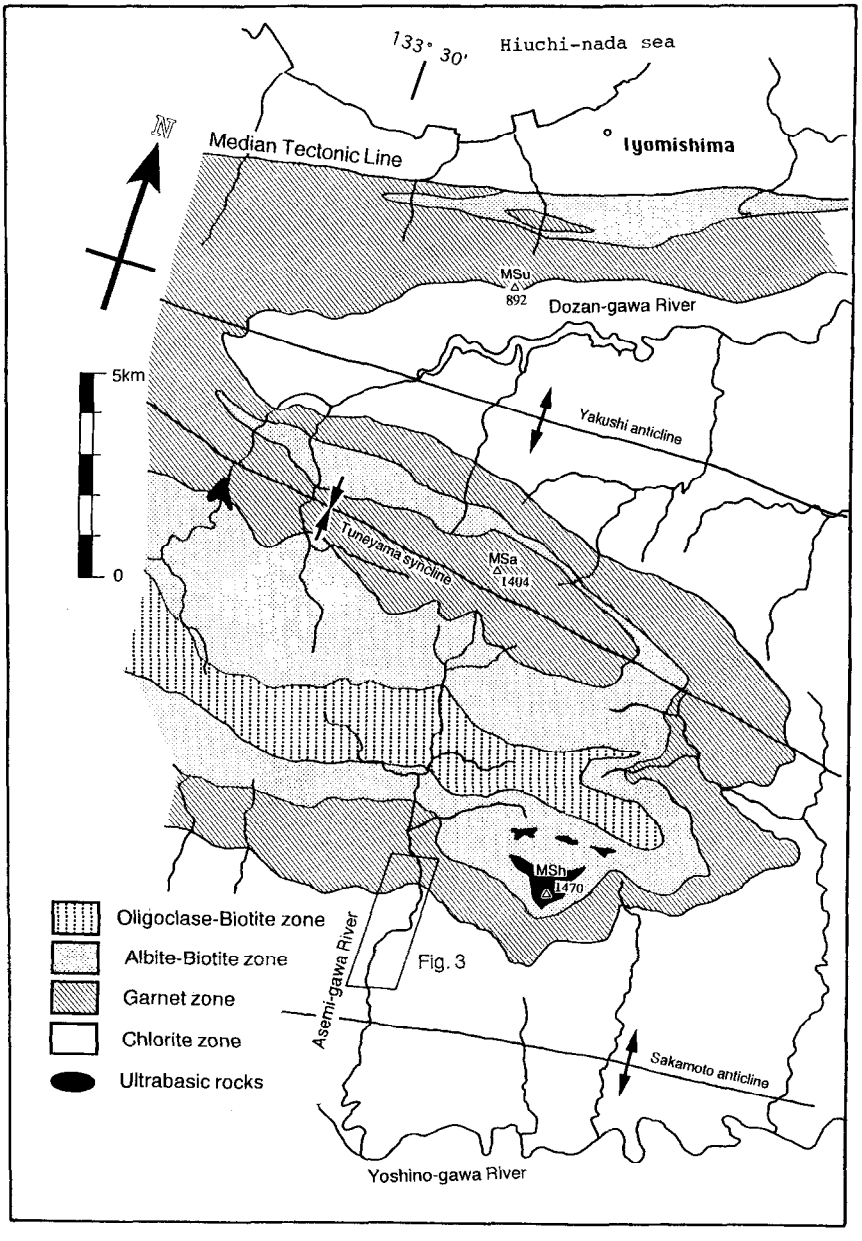

Fig. 2. The distribution of metamorphic zones and large scale D_3 fold axes in central Shikoku (compiled from the data by Higashino, 1990; Hara *et al.*, 1992; Hara and Shiota, 1996). A box marks the region of Fig. 3. MSu: Mt. Suiha-mine, MSa: Mt. Sazareo-yama, MSh: Mt. Shiraga-yama.

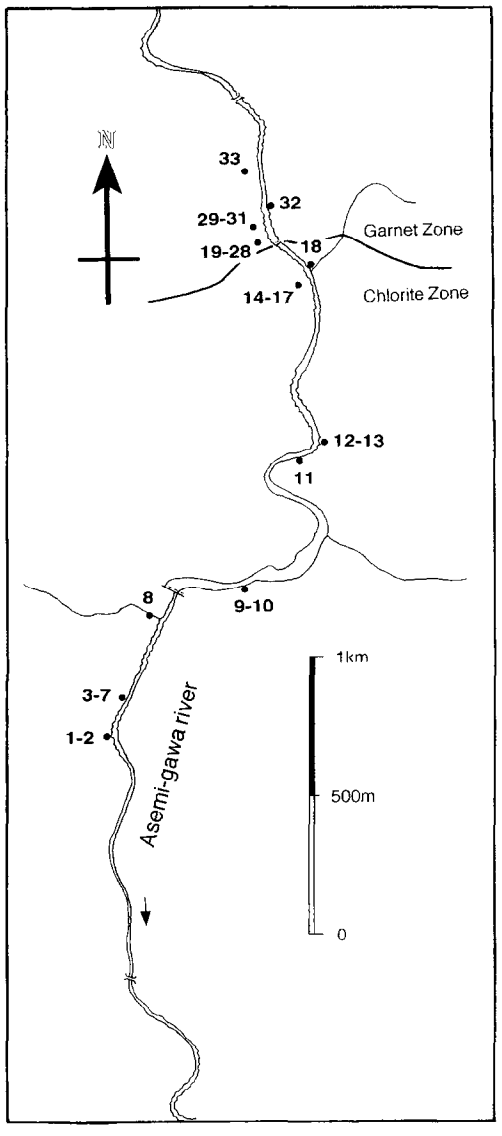

Fig. 3. Sampling localities in the Asemi-gawa river region. Samples have been numbered in structurally ascending order. Hyphenated sample numbers indicate that more than one sample was collected within one or adjacent localities.

nar schistosity (S_1) in order to eliminate the influence of these later phase deformations. All the samples were numbered in the structural ascending order (Fig. 3). In quartz schist layers thicker than several meters, samples were collected every 20–30 cm perpendicular to S_1. The successive sample numbers shown in Fig. 3 indicate the localities where several samples were analyzed.

Two orthogonal thin sections (XZ and YZ) were prepared from the samples; X is parallel to L_1, Z is normal to S_1, and Y is normal to both the X and Z axes (Fig. 4a). Some photomicrographs are shown in Fig. 5. In the XZ section, recrystallized quartz grains are notably elongate parallel to X in all the samples. Large size grains exhibit various intragrain deformation structures, such as undulatory extinction and subgrain boundaries, but rarely show deformation lamellae. The shape of these grains is approximated to be ellipsoidal. The actual grain boundaries, however, are serrated and nuclei developed at the margin of the grains (Fig. 5g). Small and relatively equant grains formed at the boundaries of larger grains are often free from these intracrystalline deformation features. Similar microstructures have also been reported by Masuda (1982) for samples collected from the same area (Area II after Masuda, 1982).

DATA ACQUISITION AND DATA ANALYSIS

Grain dimension (length of the long and short axes; a, b) and angle (Φ) between the trace of S_1 and long axis in the recrystallized quartz grains have been measured in both the XZ and YZ sections directly under optical microscope. Thin sections are set on a mechanical stage, and the magnification of microscope is set to be ×40 throughout the measurements for all the samples to avoid the bias arising from the measurement by different magnifications. The gypsum plate is also used to accurately identify the quartz grain boundaries. From these measurements, size (d)

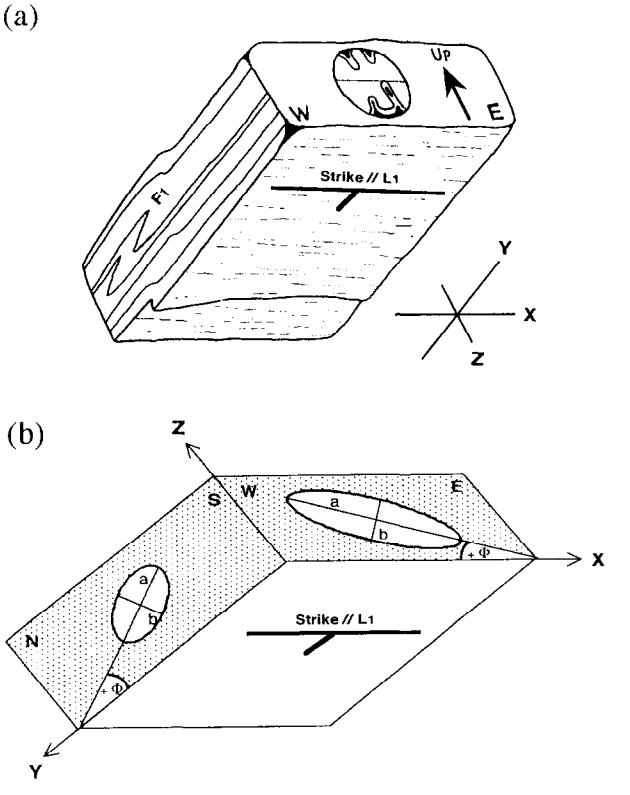

Fig. 4. (a) Schematic drawing of a hand specimen which shows the kinematic framework defined in this study. Strike and dip symbols are shown on the lower part of the sample. Principal finite extension (X) direction is taken parallel to the mineral stretching lineation (L_1), which trends east–west and horizontal in the studied area. Schistosity (S_1//XY plane) is commonly folded by F_1 intrafolial folds, the axial planes of which are parallel to S_1. A schematic c-axis fabric diagram is shown in the XZ section. (b) Shape parameters a, b and $+\Phi$ are illustrated in schematic recrystallized quartz grains.

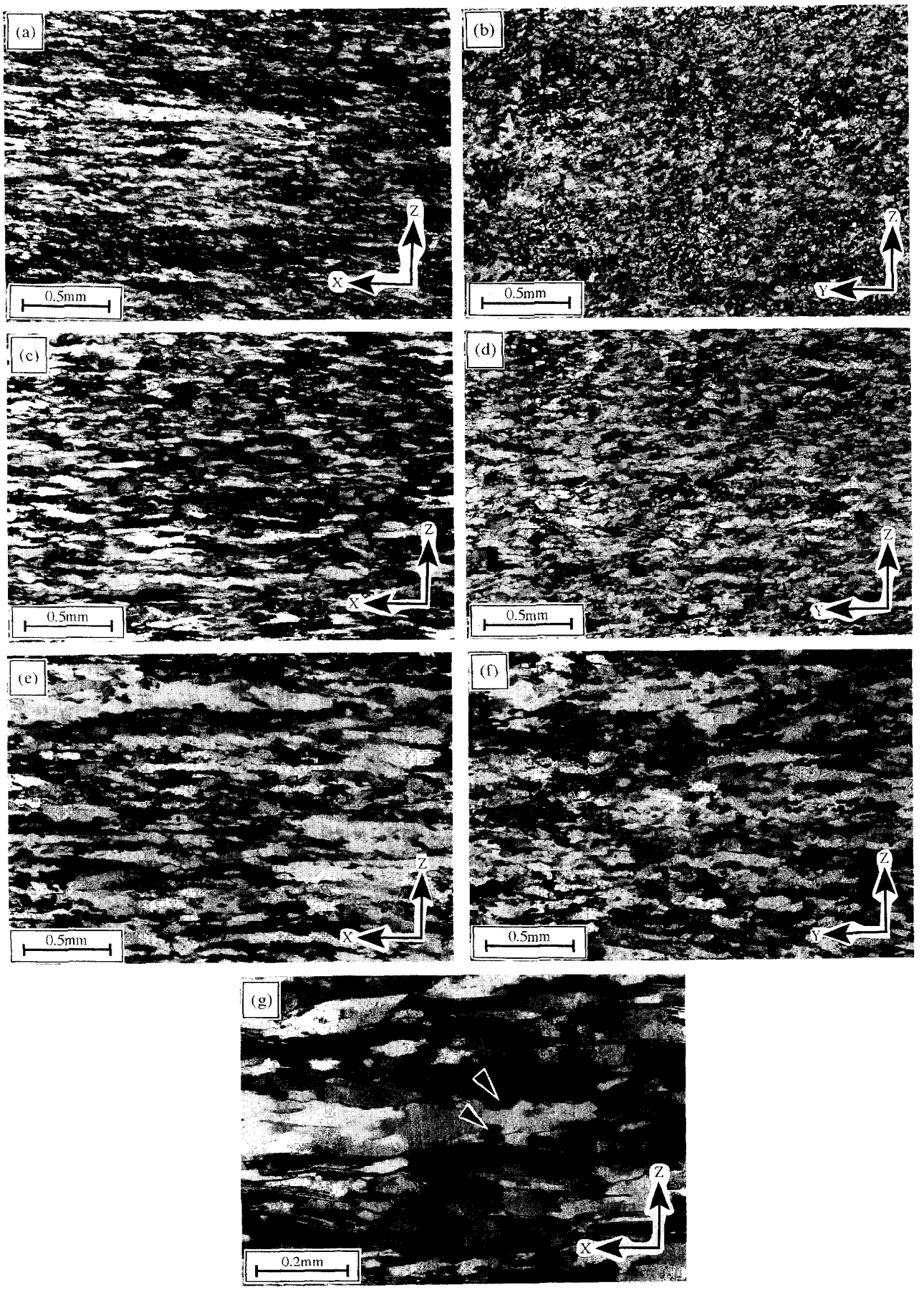

Fig. 5. Photomicrographs of Sambagawa quartz schists. All the photomicrographs were taken under crossed polarizers. X, Y and Z axes have been defined in Fig. 4(a). (a) XZ section of sample 4. (b) YZ section of sample 4. (c) XZ section of sample 12. (d) YZ section of sample 12. (e) XZ section of sample 21. (f) YZ section of sample 21. (g) Development of subgrain boundaries and neoblast (arrows) in an elongated grain in the XZ section of sample 23.

and aspect ratio (R) of each grain are defined as

$$d = \sqrt{ab} \tag{1}$$

$$R = \frac{a}{b}, \tag{2}$$

where Φ is taken as 0° when the long axis of the grain is parallel to the X/Y direction, and positive if it dips eastward/northward in XZ/YZ section (Fig. 4b). One hundred and forty measurements were carried out for both the XZ and YZ sections of all the samples, and the arithmetical mean was calculated for each sample (D, R_{xz}, R_{yz}).

From the acquired mean aspect ratios for both the XZ and YZ sections (R_{xz}, R_{yz}), grain shape k-value and strain magnitude parameter $\bar{\varepsilon}_s$ (Nadai, 1963; assuming no volume change) have been determined as follows

$$k = \frac{R_{xz}/R_{yz} - 1}{R_{yz} - 1} \tag{3}$$

$$\bar{\varepsilon}_s = \frac{1}{\sqrt{3}}\left(\left(\ln\left(R_{xz}/R_{yz}\right)\right)^2 + \left(\ln R_{yz}\right)^2 + \left(\ln R_{xz}\right)^2\right)^{\frac{1}{2}} \tag{4}$$

In each sample the c-axis orientations of 350 recrystallized quartz grains have been measured with a universal stage. Projected c-axis orientation distribution in equal area nets is contoured using the stereonet program by Allmendinger (1988), and the normalized eigenvalues of orientation tensors (Woodcock, 1977) of the c-axis fabrics, S_i (i = 1,2,3) were calculated. Fabric intensity I (Lisle, 1985) is defined by

$$I = \frac{15}{2}\sum_{i=1}^{3}\left(S_i - \frac{1}{3}\right)^2. \tag{5}$$

Notations of the parameters described above are listed in Table 1.

Table 1. Notation

Term	Meaning
a	length of grain long axis
b	length of grain short axis
Φ	angle between long axis of quartz grain and schistosity
d	size of each grain
D	mean grain size in XZ section
R	aspect ratio of each grain
R_{xz}	mean aspect ratio in XZ section
R_{yz}	mean aspect ratio in YZ section
$\bar{\varepsilon}_s$	strain magnitude (Nadai, 1963)
k	k-value
S_i	normalized eigenvalues of the orientation tensor of c-axis fabric
I	fabric intensity (Lisle, 1985)

RESULTS

c-Axis fabric

Figures 6–8 display c-axis fabric diagrams of all the collected samples (sample numbers are the same as those in Fig. 3 & Table 2). Measured c-axis fabrics can be grouped into three girdle patterns: cleft girdles, type I crossed girdles (Lister *et al.*, 1978) and small circle girdles.

(1) Cleft girdles. All the samples which show this c-axis fabric pattern (samples 1–10) were collected from the southernmost part of studied area (Fig. 3). The patterns are characterized by symmetrically disposed 65–75° small circle girdles around the X axis. The c-axis orientations are not uniformly distributed along the small circle girdles, but rather more densely populated near the Z direction than the Y direction (Fig. 6, samples 1–6, 8–10).

(2) Type I crossed girdles. This is the dominant c-axis fabric pattern in the analyzed samples (samples 11–15, 18, 23–31, 33). This fabric consists of symmetrically arranged 15–30° small circle girdles around the Z axis and a connecting girdle across the Y axis (Lister *et al.*, 1978). However, the c-axis concentration near the Y direction is relatively low, and the girdles are not connected in some cases (Figs 7 & 8, samples 15, 24–26, 28–31, 33), as is the case for the cleft girdle pattern.

Table 2. Measured values for the parameters of shape fabrics and c-axis fabrics in recrystallized quartz grains (see text for a full explanation about each parameter)

Sample No.	D (μm)	R_{xz}	R_{yz}	k	$\bar{\varepsilon}_s$	I
1	105	4.45	1.93	1.4	1.06	1.23
2	105	4.79	1.93	1.59	1.11	1.5
3	91	5.18	1.78	2.45	1.18	1.39
4	101	5.64	2.09	1.56	1.23	1.37
5	111	5.56	1.9	2.14	1.23	1.33
6	106	3.94	1.68	1.98	0.98	1.04
7	104	5.27	2.03	1.55	1.18	0.86
8	100	4.86	1.85	1.91	1.13	0.94
9	124	4.78	1.94	1.56	1.11	1.5
10	90	5.94	1.97	2.08	1.27	2.06
11	128	4.67	2.43	0.64	1.09	0.59
12	115	5.92	3.29	0.35	1.28	0.83
13	124	4.49	2.5	0.53	1.07	0.59
14	118	3.8	2.47	0.37	0.96	0.69
15	113	5.25	2.49	0.74	1.17	0.9
16	111	6.01	2.87	0.59	1.27	1.39
17	105	4.7	3.43	0.15	1.16	1.25
18	127	4.62	2.8	0.36	1.1	0.48
19	114	5.02	3.89	0.1	1.23	1.25
20	115	4.35	4.01	0.03	1.17	1.23
21	109	4.36	3.89	0.04	1.16	1.49
22	125	5.81	4.07	0.14	1.32	1.77
23	124	5.81	3.01	0.46	1.26	0.92
24	113	5.42	2.61	0.67	1.2	0.82
25	116	5.33	3.16	0.32	1.21	1.12
26	113	5.42	2.73	0.57	1.2	0.95
27	118	4.96	2.99	0.33	1.16	1.06
28	121	4.68	2.85	0.35	1.11	1.07
29	119	3.33	2.27	0.37	0.87	0.6
30	116	3.03	2.2	0.31	0.81	0.73
31	135	3.27	2.47	0.22	0.88	0.58
32	122	4.72	3.3	0.24	1.14	0.94
33	130	4.47	2.49	0.53	1.07	0.65

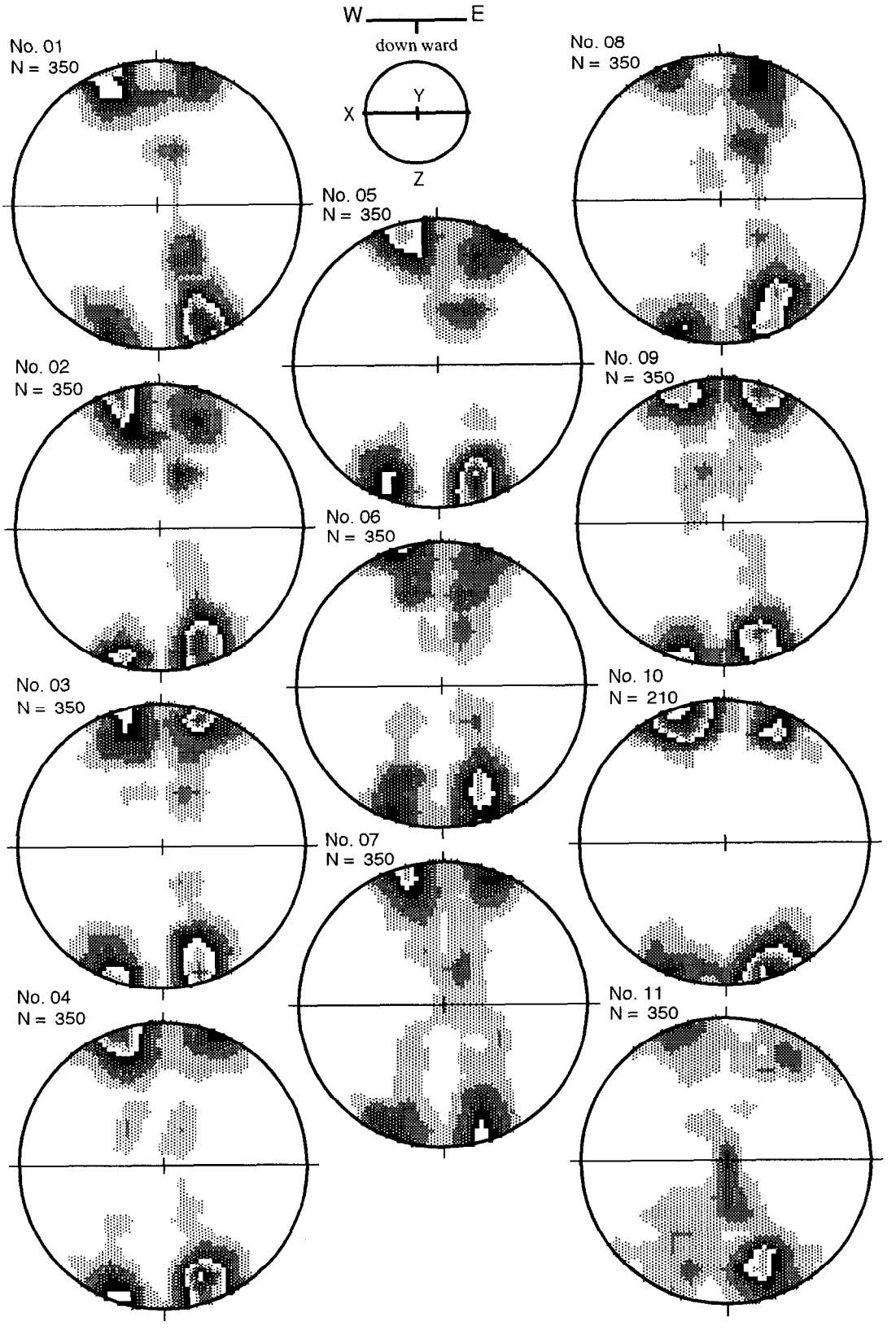

Fig. 6. Quartz *c*-axis fabrics of samples 1–11 (sample numbers are indicated in the upper-left corner of each diagram). All the *c*-axis fabrics have been plotted using the stereonet program by Allmendinger (1988). Upper-hemisphere, equal-area projections viewed towards the north (i.e. in *XZ* sections). East–west oriented solid line denotes foliation. See legend for the sample coordinate system. Contour interval is 1% per 1% area and lowest contour is 1% per 1% area. *N* is the number of measured *c*-axis orientations.

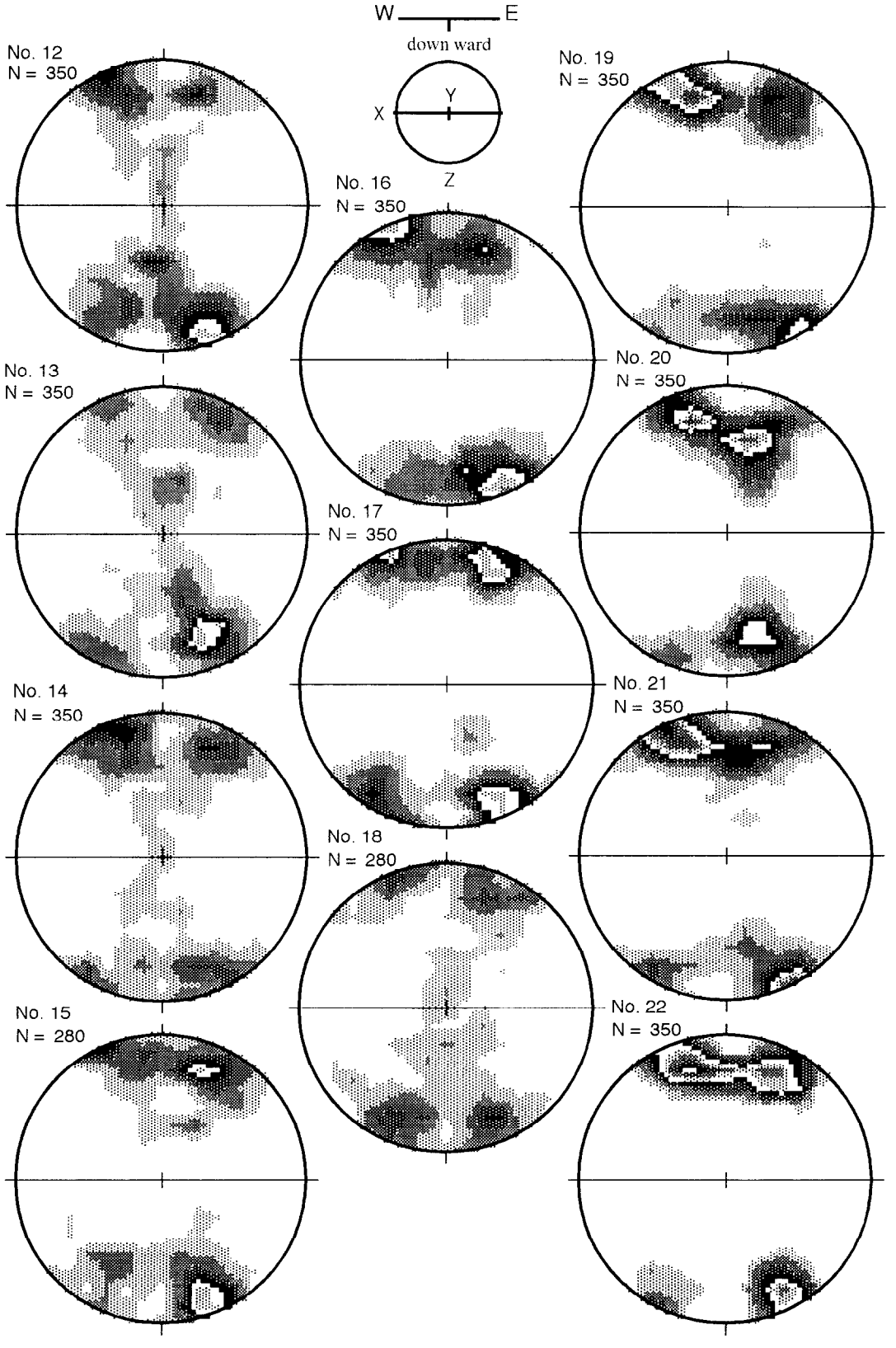

Fig. 7. Quartz *c*-axis fabrics of samples 12–22. See caption in Fig. 6 for full explanation.

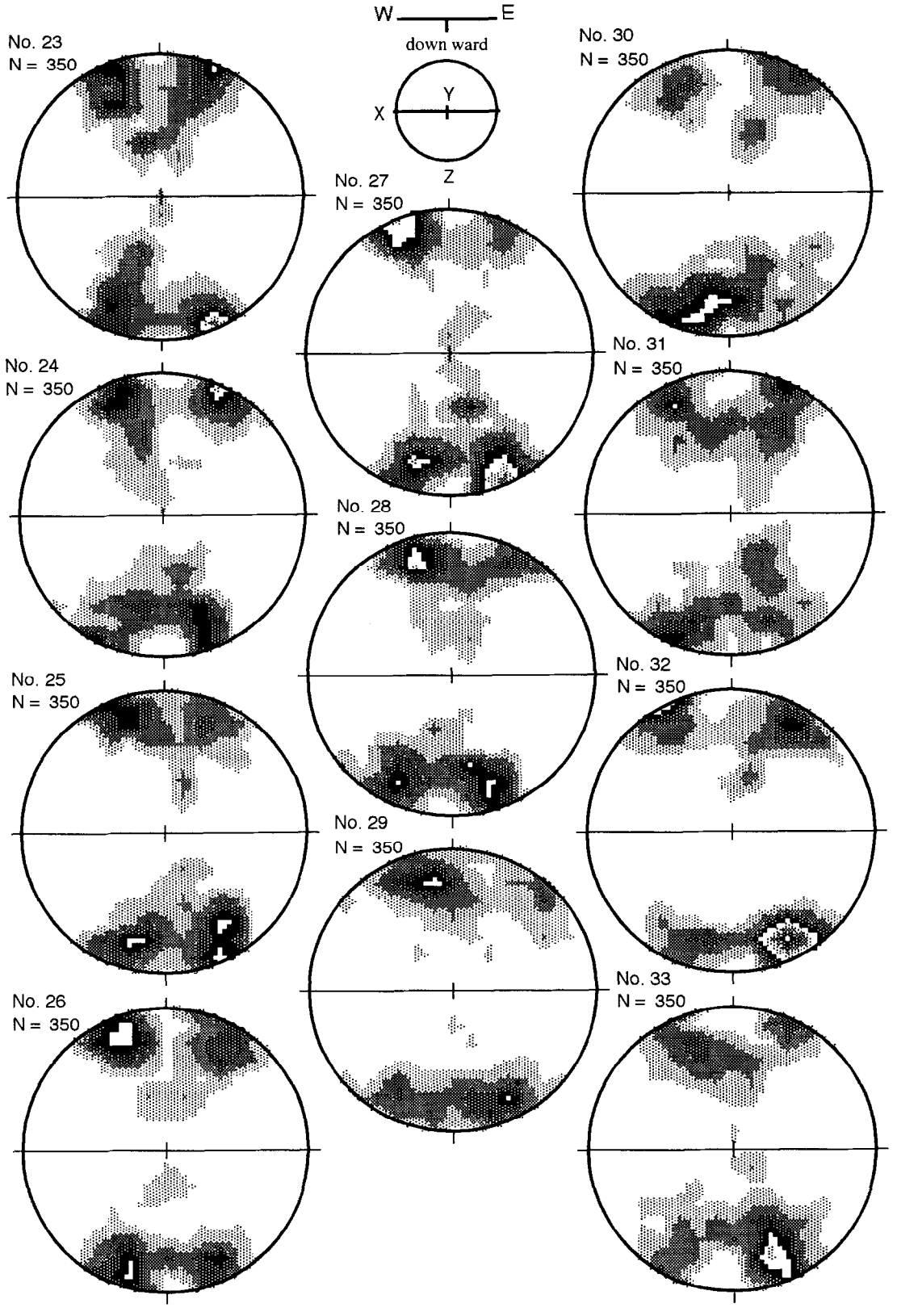

Fig. 8. Quartz c-axis fabrics of samples 23–33. See caption in Fig. 6 for full explanation.

(3) Small circle girdles. The girdle patterns of this type were observed in seven samples (samples 16, 17, 19–22, 32), which were collected near the boundary between the chlorite zone and garnet zone (Fig. 3). The girdles are characterized by symmetrically dispersed 20–40° small circles centered on the Z axis, although a lack of c-axis concentration occasionally occurs in some parts of the girdle (e.g. Fig. 7, sample 22).

In spite of the variety of c-axis fabric patterns, the half opening angles of the girdle patterns from the Z axis are fairly uniform (15–40°) in all the samples. The symmetry of the fabric skeletons is nearly orthorhombic, and the symmetry axes conform well to the meso-

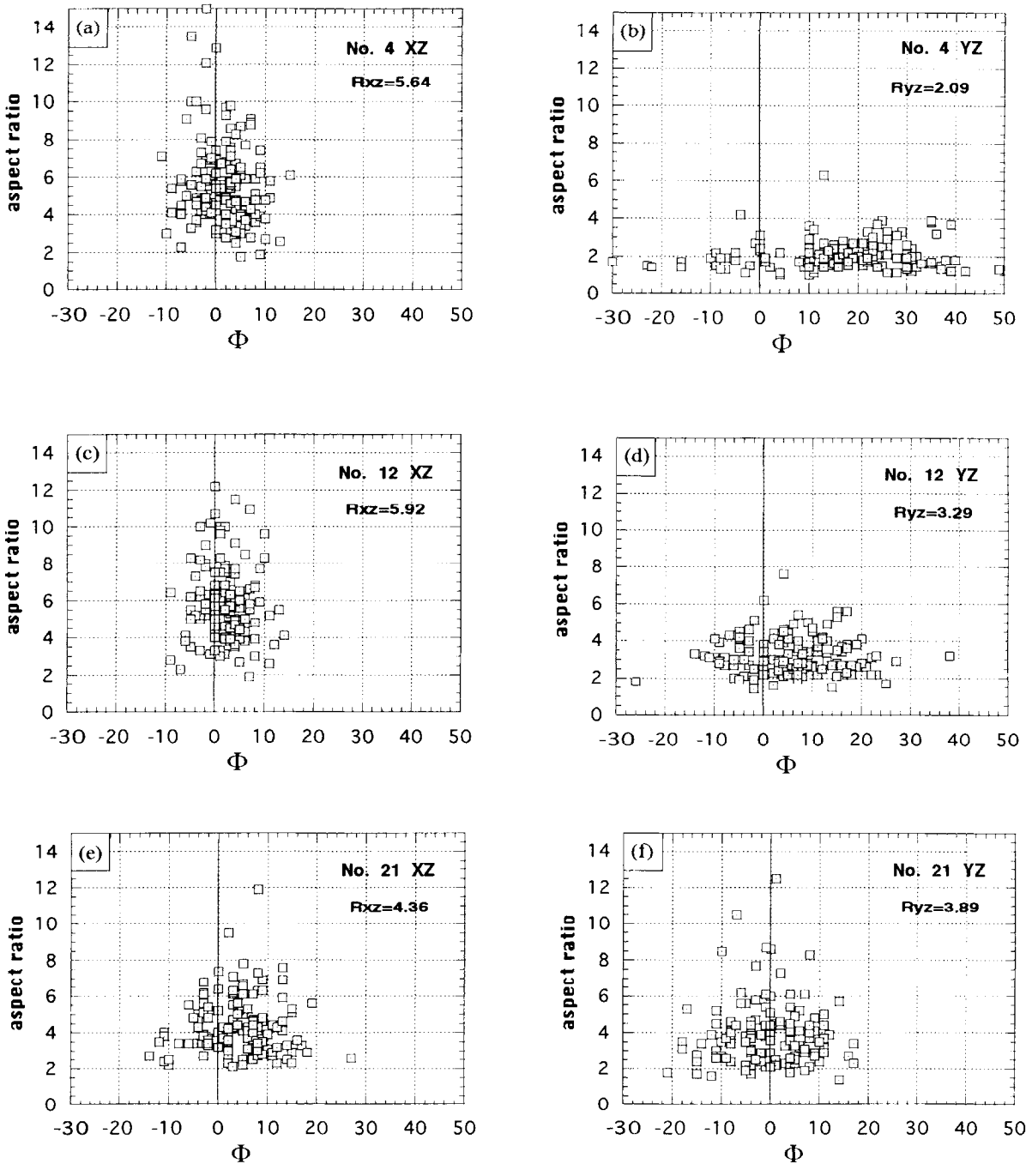

Fig. 9. R–Φ diagrams in both the XZ and YZ sections of three samples (sample numbers are indicated in the upper-right corner of each diagram), which correspond to the samples for Fig. 5 (photomicrographs). Note the similar shape fabrics of recrystallized quartz grains in XZ sections, while those in YZ sections vary among the three samples. The mean aspect ratio in each section is indicated in the upper right corner of each diagram.

scopic kinematic framework (i.e. S_1 and L_1) in all the samples.

Grain shape fabric

Table 2 shows all the measured values for the parameters of grain shape and c-axis fabric. Mean grain size, D is about 90–120 μm in the southern part of the studied region (samples 1–13), and about 110–130 μm in the northern part (samples 14–33), and generally increases with increasing peak metamorphic grade. However, D seems to also be affected by the volume fraction of accessory minerals.

The k-values in the samples calculated from the mean aspect ratios in both the XZ and YZ sections vary greatly between 0 and 2.5. This fact is well represented in photomicrographs (Fig. 5) and R–Φ diagrams of three representative samples (Fig. 9). Figure 5 shows that the aspect ratios in the XZ section are generally high (Fig. 5a, c & e), while those in the YZ sections are variable among the samples (Fig. 5b, d & f). R–Φ diagrams in the XZ sections (Fig. 9a, c & e) are all similar, and show more or less symmetrical distribution with respect to $\Phi = 0$ (parallel to the X direction) with the highest aspect ratio near $\Phi = 0$ and a narrow range of Φ ($-10^\circ \leq \Phi \leq 10^\circ$). However, there is a distinctive difference in the R–Φ diagrams in the YZ sections. The R–Φ diagram in the YZ section of sample 4 (Fig. 9b) shows a lack of shape preferred orientation in addition to a low mean aspect ratio ($R_{yz} = 2.09$), while that of sample 21 (Fig. 9f) exhibits a high mean aspect ratio ($R_{yz} = 3.89$) and a narrow range of Φ around $\Phi = 0$, as well as in the XZ section. These data, together with the photomicrographs in the two orthogonal sections, support the conclusion that different samples are characterized by different three-dimensional grain shapes.

Figure 10 shows the relation between the aspect ratio and recrystallized grain size (R d diagram) of each grain in three samples. There is essentially no correlation between them and no detailed relation has been derived from these diagrams. In order to fully examine the relation between the recrystallized grain size and shape fabrics, R–Φ diagrams have been reconstructed separately for the different classes of recrystallized grain size (Fig. 11). The R–Φ distributions for the three different classes of recrystallized grain size are more or less similar, and therefore similar to the bulk distribution of R Φ diagrams in the XZ section.

Relationship between the c-axis fabric and grain shape fabric

The relationship between c-axis fabric patterns and recrystallized quartz grain shape is as follows. A Flinn (1962) diagram (Fig. 12) summarizes the relation between c-axis fabric patterns and k-values of the grain shape. In Fig. 12, the symbol of scatter points differs according to the three different girdle patterns of c-axis fabrics. The figure reveals a distinct correlation between k-values and c-axis fabric patterns for all the samples, namely the same symbols are clustered in particular regions. Samples which show cleft girdle c-axis fabric patterns are characterized by relatively high k-values (1.5–2.5). Type I crossed girdle c-axis fabrics typify the samples where k-values vary between 0.3 and 0.6. It should be noted that some samples with

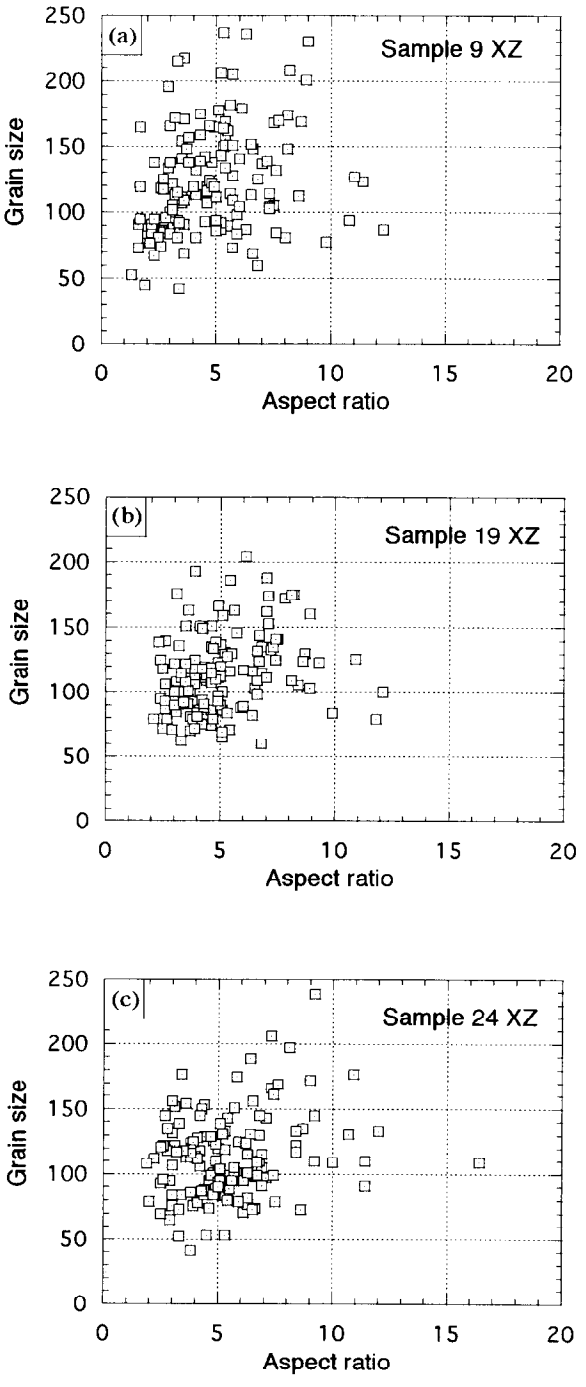

Fig. 10. R–d diagrams (two-dimensional scatter diagram which shows the relation between the aspect ratio and recrystallized grain size of each grain) in the XZ sections for three samples (sample numbers are indicated in the upper-right corner of each diagram).

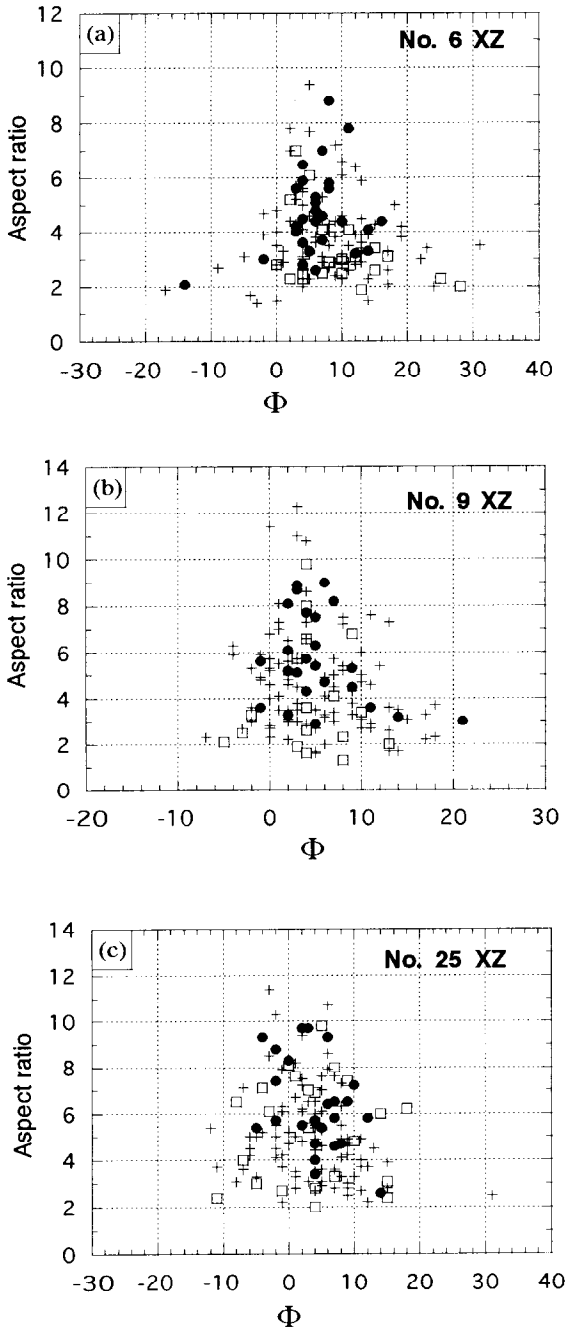

Fig. 11. Reconstructed R Φ diagrams for the different classes of recrystallized grain size in three samples (sample numbers are indicated in the upper-right corner of each diagram). Scatter symbols are changed according to the three classes of recrystallized grain size, i.e. larger size than the mean size plus one standard deviation (σ) (filled circle), intermediate size within the mean size $\pm\sigma$ (cross) and smaller size than the mean size minus σ(open square).

relatively high k-values (0.46–0.67 in samples 23–24, 26) show a transitional c-axis fabric pattern between type I crossed girdles and cleft girdles. Samples with relatively low k-values (close to 0.3) show a typical type I crossed girdle pattern. The k-values for samples with small circle girdle c-axis fabric patterns are generally very low (<0.2), although sample 16 shows an exceptionally high k-value (0.59).

Figure 13 summarizes the relationship between the strain magnitude $\bar{\varepsilon}_s$ calculated from the mean aspect ratios of recrystallized grains, and fabric intensity I calculated from the eigenvalues of the orientation tensor of c-axis fabrics. For each of the different strain geometries, the relationship shows a rough proportionality (enclosed by ellipses), although the factor of proportionality is different. In order to closely investigate the relationship, four samples (samples 29, 14, 27 and 25) which exhibit similar c-axis fabric patterns (type I crossed girdles) and k-values were selected where the strain magnitude gradually increases from sample 29 to 25. We have investigated the change in c-axis fabrics and R–Φ diagrams with increasing strain magnitude $\bar{\varepsilon}_s$ (Fig. 14). The small circle girdles around the Z axis become firm with increasing $\bar{\varepsilon}_s$ values, which is reflected in the increasing values of fabric intensity I. Furthermore, their R–Φ distribution also progressively changes with the calculated strain magnitude $\bar{\varepsilon}_s$. Samples 29 and 14 with lower $\bar{\varepsilon}_s$ values, show relatively low aspect ratios (2–7) with Φ values greatly varying from -15° to 25°. On the other hand, samples 27 and 25 with higher $\bar{\varepsilon}_s$ values show relatively high aspect ratios (2–11) with Φ values mostly concentrating between -10° and 15°.

We have briefly examined the c-axis preferred orientation as a function of size and shape of recrystallized grains in the same sample. For samples 19 and 24, we measured the c-axis orientations in relatively fine recrystallized grains ($<100\ \mu$m) with low aspect ratios (<2 in XZ section), together with those in randomly selected grains (Fig. 15). The fraction of the fine equant grains is less than a few percent of the randomly selected grains. Although the c-axis fabric patterns show similar skeletons in both the randomly selected and fine equant grains, the degree of concentration is weaker and hence the intensity parameter I is lower in the fine equant grains than in the randomly selected grains. Furthermore, the position of maximum concentration of c-axis orientation is different for the randomly selected and fine equant recrystallized grains. For example, in sample 19, although the c-axis orientations in randomly selected grains are mostly concentrated in an eastward dipping direction within the small circle girdles, those of fine equant grains are mostly concentrated in a westward dipping direction within the same small circle girdles, which is the orientation of secondary maximum in the former pattern. Since the asymmetry of c-axis fabric pattern in the randomly selected grains suggests a top to the west sense of shear, the former and latter c-axis maxima are well and less favorably oriented for basal (0001) slip, respectively.

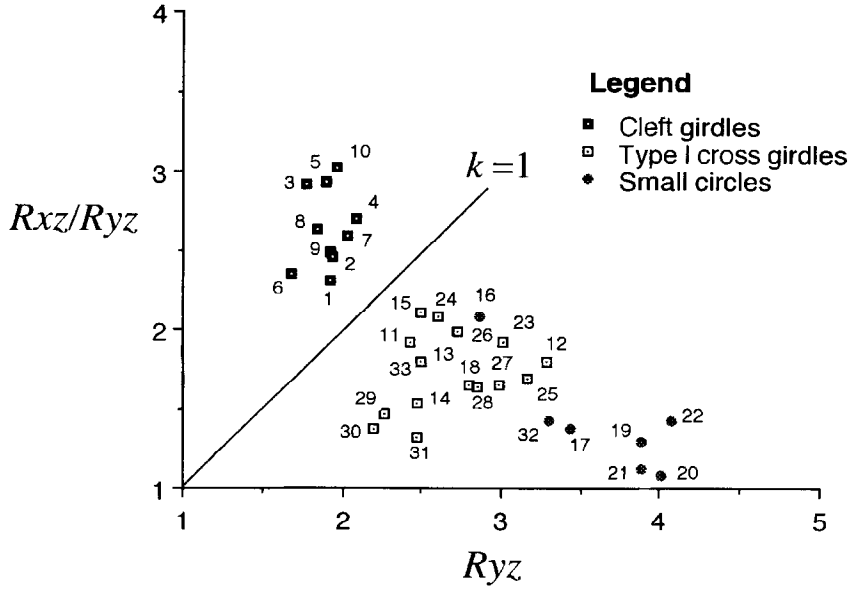

Fig. 12. Flinn (1962) diagram of the average shapes of recrystallized quartz grains. Symbols differ according to the three types of quartz c-axis fabrics (see legend). The number next to each symbol denotes sample number.

DISCUSSION AND CONCLUSIONS

Origin of quartz c-axis fabrics and inferred deformation conditions

The c-axis fabrics observed in the present study are type I crossed girdles, cleft girdles and small circle girdles with small half opening angles (*ca* 15–40°). Similar c-axis fabrics have been recognized in quartz schists from the Sambagawa metamorphic belt (e.g. Kojima and Hide, 1957, 1958; Oyagi, 1964; Sakakibara *et al.*, 1992; Wallis *et al.*, 1992). The c-axis fabrics observed in the present samples can be reproduced by the Taylor model quartzite B of Lister and Hobbs (1980) (also see Price, 1985). This fact suggests that the development of the observed c-axis fabrics was perhaps caused by intracrystalline slip in quartz and controlled by the kinematics of plastic flow in the samples. The active slip systems in model quartzite B are basal $<a>$, rhomb $<a>$ and rhomb $<a + c>$ (Lister and Hobbs, 1980), which are in fact proven to have been active in natural quartzite deformed under greenschist facies conditions, based on the crystallographic orientations of the rotation axis of misorientation in recrystallized grains (or subgrains) (e.g. Lloyd and Freeman, 1991, 1994; Fliervoet and White, 1995). Nevertheless, the activity of rhomb $<a + c>$ could have been limited in natural quartz schist because of the high critical resolved shear stress (e.g. Trépied and Doukhan, 1982). The kinematically controlled c-axis fabrics are also supported by the fact that the c-axis fabric intensity increases with increasing strain magnitude in the present samples (Fig. 13).

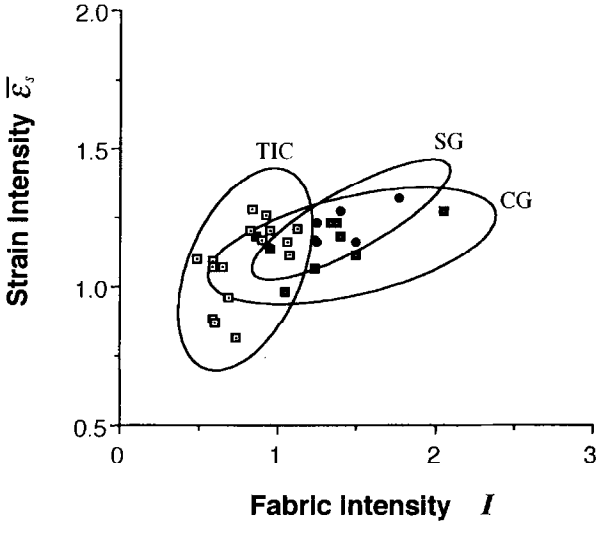

Fig. 13. Correlation between the strain magnitude $\bar{\varepsilon}_s$ calculated from the mean aspect ratios of recrystallized quartz grains in *XZ* and *YZ* sections, and fabric intensity *I* calculated from the normalized eigenvalues of orientation tensor of c-axis fabric. Symbols are same as those in Fig. 12. For each of the different c-axis fabric patterns indicative of different strain geometries, the relationship shows a rough proportionality (enclosed by ellipses). TIC; type I crossed girdles, SG; small circle girdles, CG; cleft girdles.

In natural quartzites deformed under greenschist conditions, it has also been demonstrated that dynamic recrystallization predominantly occurred by progressive subgrain rotation (e.g. Bouchez, 1977; Law, 1987) in which the crystallographic orientations of recrystallized grains are controlled by those of parent grains (e.g. Guillope and Poirier, 1979) and hence the kinematically induced LPO does not change much. In the present study, it has been noted that the c-axis fabric skeletons in the randomly selected and fine equant grains in some samples are similar (Fig. 15): the crystallographic orientations in the nucleated fine grains mimicked those in the parent grains. Therefore, we conclude that in the present samples dynamic recrystallization occurred dominantly by subgrain rotation, and

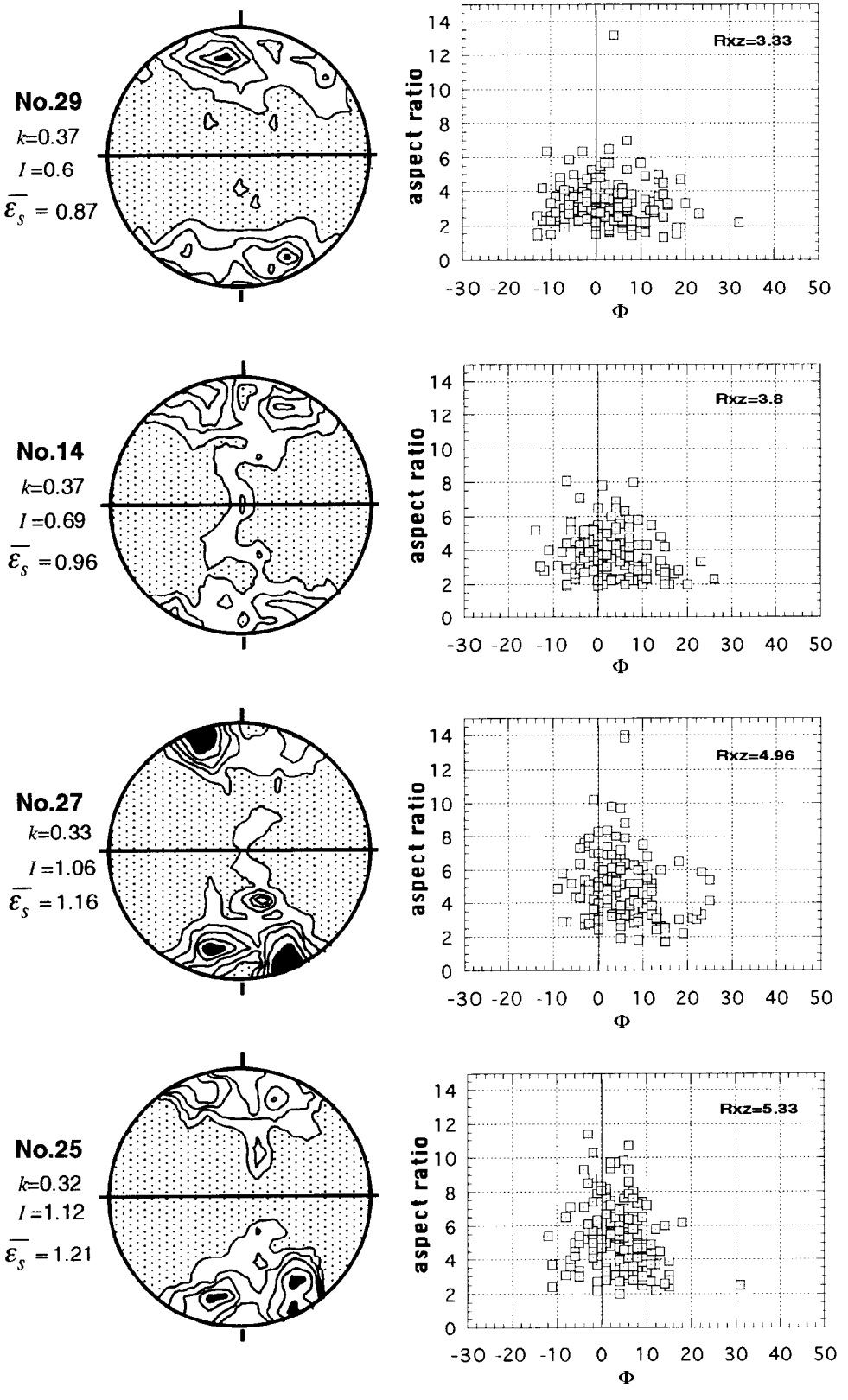

Fig. 14. Variation of both c-axis fabric and R–Φ diagram in XZ section with increasing strain magnitude $\bar{\varepsilon_s}$ in four samples exhibiting similar k-values. Sample numbers, k-values, fabric intensity I and strain magnitude $\bar{\varepsilon_s}$ are indicated at the left hand side of each c-axis diagram, while mean aspect ratio in XZ section (R_{xz}) is indicated in the upper-right corner of each R–Φ diagram. Contour interval is 1% per 1% area and lowest contour is 1% per 1% area. Dotted regions are below 1%, and black above 5% per 1% area.

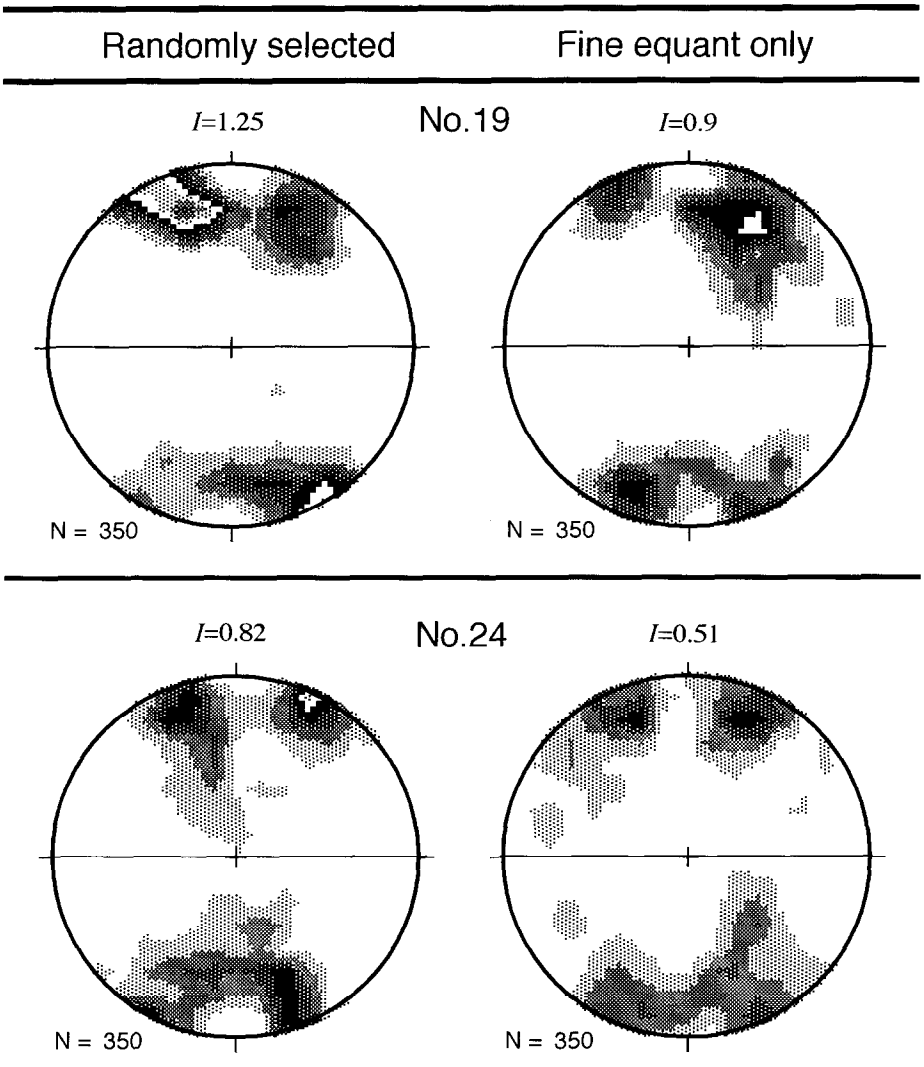

Fig. 15. Difference in c-axis fabric between randomly selected (also shown in Figs 7 & 8) and relatively fine equant ($R < 2$) grains in two samples (samples 19 and 24). The number of measured c-axis orientations (N) and fabric intensity (I) are also shown in each diagram. Contour interval is 1% per 1% area and lowest contour is 1% per 1% area.

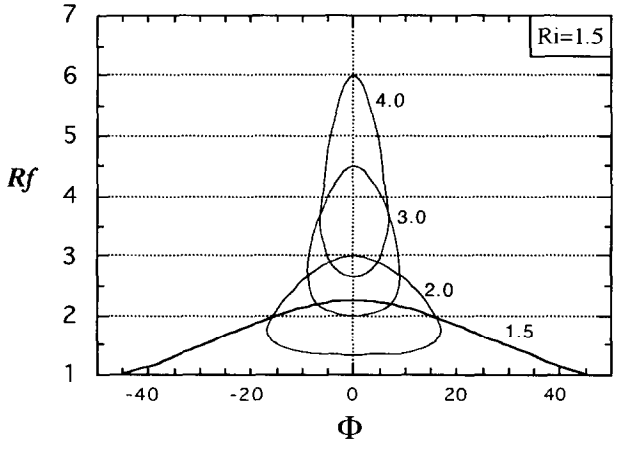

Fig. 16. Theoretically derived R_f–Φ curves for an initial aspect ratio $R_i = 1.5$ and varying values of strain ratio R_s (1.5–4) (reproduced after Ghosh, 1993).

the kinematically induced c-axis fabrics were mostly preserved regardless of the occurrence of dynamic recrystallization.

Takeshita and Wenk (1988) proposed that model quartzite B represents a quartzite deformed under greenschist conditions, and later Takeshita (1996) has concluded that the c-axis fabrics corresponding to model quartzite B could have been formed at the temperature conditions of 300–400°C from a review of previous studies. If these temperature conditions are valid for the present samples, the deformation of quartz schist is inferred to have taken place at lower temperatures than the peak metamorphic temperatures in the garnet zone, which has been petrologically inferred to have been *ca* 450°C (Enami *et al.*, 1994). Hence, the deformation of quartz schist responsible for the development of c-axis fabrics could have occurred

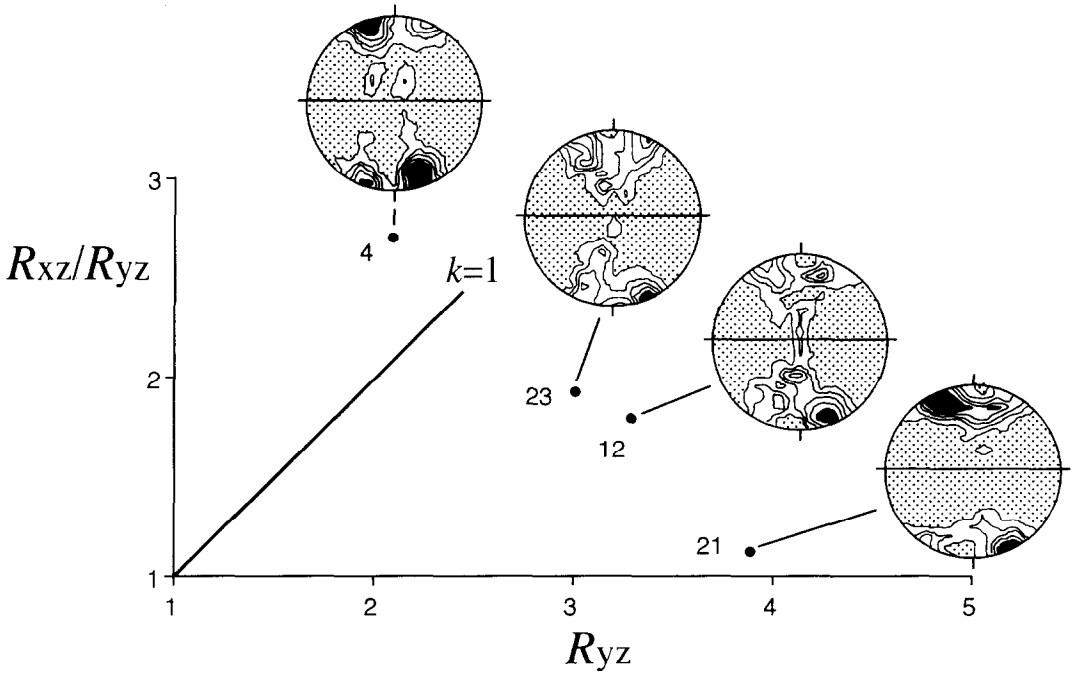

Fig. 17. Representative types of c-axis fabrics as a function of recrystallized quartz grain shape on the Flinn (1962) diagram. The number next to each c-axis fabric diagram denotes sample number. See captions of Fig. 14 for a full explanation on c-axis fabric diagrams.

under a retrograde metamorphism during the exhumation of the Sambagawa metamorphic belt.

Relationship between the quartz c-axis fabrics and grain shape fabrics

It has been noted that the R–Φ distribution in the present samples progressively changes with increasing strain magnitude $\bar{\varepsilon}_s$ (Fig. 14) which itself proportionally changes with the kinematically controlled c-axis fabric intensity (I): the aspect ratios increase and the range of Φ decreases with increasing $\bar{\varepsilon}_s$ values. Somewhat similar transitions can be seen in theoretically derived R_f–Φ curves for a constant initial aspect ratio $R_i = 1.5$ and varying values of strain ratio R_ss (1.5–4) [Fig. 16 which has been calculated from equations (10) and (11) of Ghosh, 1993]. This fact indicates that the strain has certainly affected the development of recrystallized quartz grain shape fabric (R–Φ diagram).

We have also shown that the recrystallized quartz grain shape and c-axis fabrics are well correlated in the present samples: cleft girdle, type I crossed girdle and small circle girdle c-axis fabrics developed in the recrystallized grains with prolate, oblate and uniaxially oblate shapes, respectively. The correlation between c-axis fabrics and grain shape geometries in representative samples has been schematically depicted in the Flinn (1962) diagram of Fig. 17. A similar relationship has also been reported in recrystallized quartz grains at axial parts of buckled quartz rich layers from the Sambagawa metamorphic belt (Hara, 1971). Therefore, we can conclude that the grain shape fabric of recrystallized quartz grains and the c-axis fabrics have been predominantly controlled by the finite strain.

Although the strain geometries inferred from both the recrystallized quartz grain shape and c-axis fabric are correlated, there are significant discrepancies between them. Recrystallized grains with k-values ranging from 1.5–2.5 in this study show cleft girdle c-axis fabrics (Fig. 12), while the theoretical study shows that axisymmetric cleft girdle c-axis fabrics are expected to be formed for infinite k-values (i.e. axisymmetric extension strain, e.g. Lister *et al.*, 1978). Similar discrepancy also applies to plane strain (i.e. $k = 1$) c-axis fabrics. Although the typical type I crossed girdles should theoretically appear in exact plane strain mode, the girdles in this study developed in recrystallized grains with k-values around 0.4 (Fig. 12). Therefore, the mode of finite strain inferred from the recrystallized grain shape is apparently deviated towards the flattening field, compared to those inferred from the c-axis fabric patterns (Fig. 17). How did these discrepancies arise? Several possible effects might explain these discrepancies, although we could not uniquely identify the cause.

1. The error which arises from grain shape measurements in two-dimensional sections is considerable. If the plane of section is not exactly along the long axis of the recrystallized grain, we may have underestimated the grain aspect ratio, particularly in the XZ section.
2. The discrepancy can be attributed to the difference in the timing of formation of the recrystallized grain shape and LPO. A subtle asynchronous devel-

opment of the grain shape and LPO might have resulted in the difference in mode of finite strain inferred from both the methods. The quartz c-axis fabrics might have been formed by a large (say more than 50% shortening) strain, while the shape of individual quartz grains was perhaps altered by superposed deformation and dynamic recrystallization. If the strain mode changed to the flattening field in the final stage of the deformation, the finite strain inferred from the grain shape could have been deviated toward the flattening field as compared to that inferred from the pattern of the c-axis fabric.

3. The arithmetical mean aspect ratio of recrystallized grains may overestimate the finite strain ratios, $\sqrt{(\lambda_X/\lambda_Y)}$ and $\sqrt{(\lambda_Y/\lambda_Z)}$ which must be used for the calculation of k-values. Here, λ_X, λ_Y and λ_Z denote the quadratic elongation in the X, Y and Z directions, respectively. The overestimation could be considerable, particularly in the YZ section. When the strain ratio R_s is lower than 2, the theoretical R_f–Φ curves exhibit a great variation of Φ (Fig. 16). The theoretical R_f–Φ curve for $R_i = 1.5$ and $R_s = 1.5$ is somewhat similar to the R–Φ diagram in YZ section for sample 4, which exhibits a typical cleft girdle c-axis fabric (Fig. 9b). If we adopt a value of $R_{YZ} = 1.5$ instead of the mean aspect ratio, $R_{YZ} = 2.1$ in sample 4, then the k-value is changed to 5.5 instead of 1.6. Therefore, the apparent deviation toward the flattening field of the strain mode, estimated from the mean aspect ratio in the two orthogonal sections, could be attributed to an overestimation of the finite strain ratio in YZ section. However, since the initial shape and orientation distribution of long axes of recrystallized grains is hard to estimate, it is essentially impossible to infer the strain ratio based on the R–Φ diagram.
4. Grain boundary migration could also explain the discrepancy. Lobate and serrated grain boundaries, and left-over grains (after Jessell, 1987) are often observed in the samples. A great amount of grain boundary migration could completely modify the shape of recrystallized grains. Deformation experiments on quartzites have shown that grains with high aspect ratios develop at relatively low temperature and high strain rate conditions, and thus at high differential stress conditions (e.g. Masuda and Fujimura, 1981; Hirth and Tullis, 1992). Karato and Masuda (1989) have inferred that the observed high aspect ratios in experimentally deformed and recrystallized quartz grains (S-type microstructure after Masuda and Fujimura, 1981) under high stress conditions can be attributed mostly to anisotropic fluid-assisted grain boundary migration (i.e. growth). The microstructures observed in the XZ section in the analyzed samples are also similar to S-type microstructure after Masuda (1982). However, Tagami (1998) found that dominant grain boundary migration in samples from the biotite zone in the Sambagawa metamorphic belt reduces the aspect ratios of recrystallized grains and weakens the grain shape fabric. This fact indirectly supports the conclusion that both the c-axis fabrics and grain shape fabrics were primarily controlled by the finite strain during deformation in the present samples.

Processes of coupled deformation and dynamic recrystallization

On the basis of our observations and results, the following three stages of coupled deformation and dynamic recrystallization processes are proposed to explain the fabric development of the recrystallized grains (Fig. 18).

Initial stage. In the history of burial and exhumation of the Sambagawa metamorphic rocks, recrystallized quartz grains might have attained their largest size with polygonal shape due to static grain growth at peak metamorphic conditions, although there is essentially no way to infer the initial microstructures before D_1. Based on the fact that the recrystallized quartz aggregates which we observe now show well defined c-axis fabrics without any fabric components indicative of pre-D_1 deformations, the c-axis fabrics of the aggregates might have been fairly random before D_1.

Deformation and the subgrain rotation recrystallization stage. As D_1 deformation progressed under greenschist facies conditions (discussed in the preceding section), strain accumulated which led to polygonization and rotation recrystallization in the parent grains. Hence, the grain size was significantly reduced through these processes. It has been noted that neither the R–d (Fig. 10) nor the R–Φ (Fig. 11) diagrams show any correlation between the recrystallized grain size and the shape fabric. This fact could suggest that there was a great variation in grain size before D_1 deformation progressed any further. It could also suggest that the cyclic operation of deformation and recrystallization during the D_1 stage so completely erased such a simple R–d relation that the larger relict grains formed at peak metamorphism are more deformed than the finer recrystallized grains formed during the D_1 stage. During D_1 deformation, the c-axis in each recrystallized grain was rotated by intracrystalline slip toward an end orientation in the girdle which was controlled by the mode of finite strain (Lister and Hobbs, 1980). The recrystallized grains of different size, shape and initial orientation of grain long axis were deformed into various shapes and passively rotated, which was also controlled by the finite strain (Fig. 18, also see R–Φ diagrams).

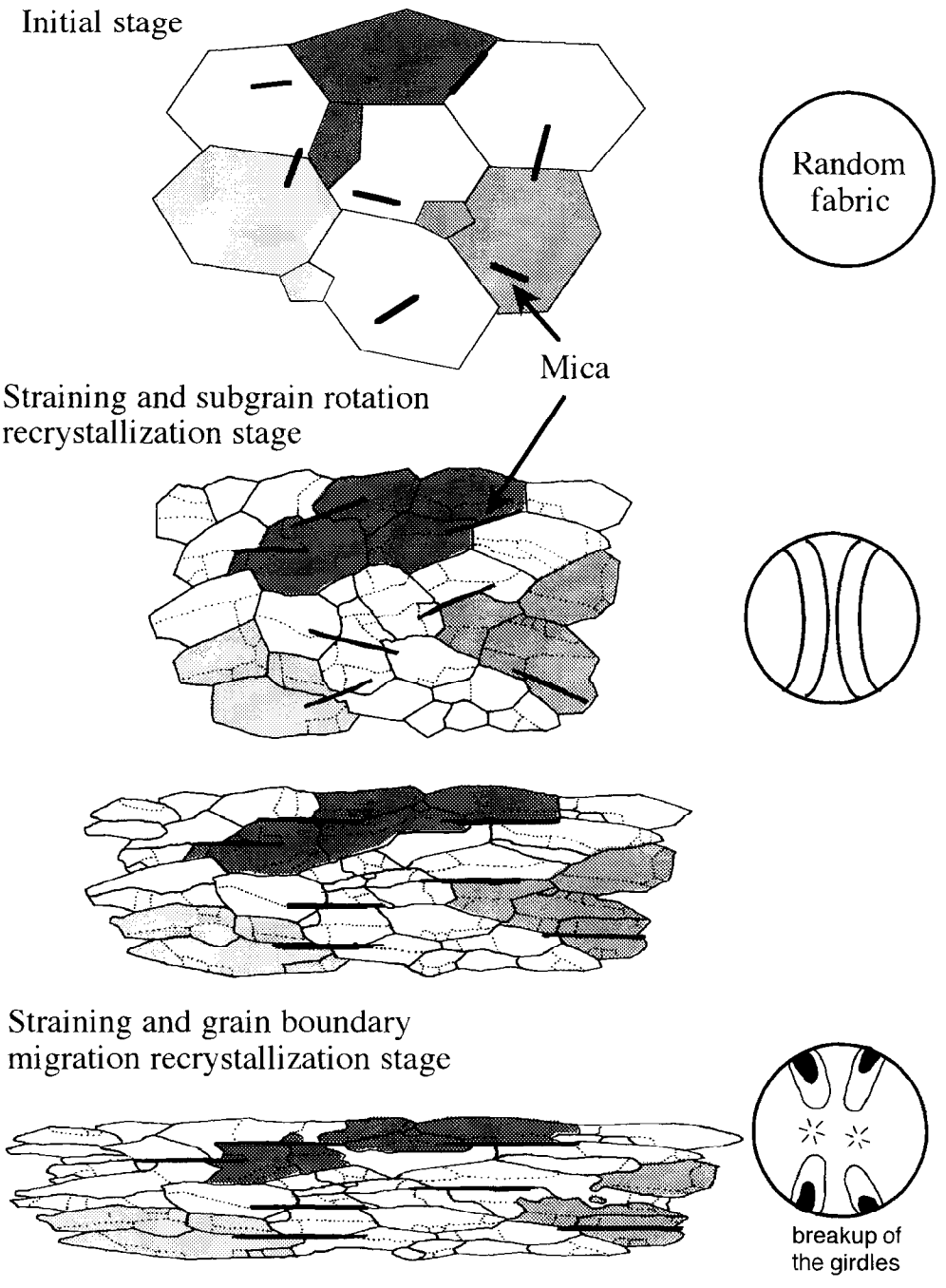

Fig. 18. Inferred microstructural development in the present samples during the processes of coupled deformation and dynamic recrystallization. Microstructural development of three domains with originally same lattice orientation is traced throughout the processes of coupled deformation and dynamic recrystallization. The development of *c*-axis fabric corresponding to each stage is also indicated.

Deformation and the grain boundary migration recrystallization stage. Once the *c*-axis orientations converged to or around the skeleton of the girdles, the grains began to harden because those *c*-axis orientations in the girdle are relatively unfavorable orientations for the activation of easy basal (0001) slip systems (geometrical strain hardening, Takeshita and Wenk, 1988). The increasing stored strain energy due to both geometrical hardening and increase of dislocation densities (hardening of slip systems) in the grains with increasing strain resulted in nucleation and growth of newly recrystallized grains, particularly at the peripheral part of these grains (Figs 5g & 18). It has been noted that the most densely populated directions of the *c*-axis fabric are different for the fine equant and randomly selected grains although the bulk *c*-axis fabric patterns are similar (Fig. 15). It is hence inferred that the grains favorably oriented for activation of easy basal (0001) intracrystalline slip could have grown by grain boundary migration at the ex-

pense of those grains which are oriented in the relatively hard crystallographic orientations (e.g. Herwegh and Handy, 1996). Consequently, those grains with *c*-axes oriented parallel to the *Y* axis [hard orientation for basal (0001) slip] could have been consumed, which resulted in breakup of the girdles (Fig. 18).

Acknowledgements—We wish to express our sincere thanks to Ikuo Hara for many stimulating discussions and comprehensive comments in the field and laboratory. Kazuhiko Ishii and Kyuichi Kanagawa substantially improved an earlier version of the manuscript and are gratefully acknowledged. We have benefited from useful comments from Tugio Shiota, Yasutaka Hayasaka, Nobuo Sakakibara and Osamu Nishikawa. During the fieldwork, the hospitality of Nobumichi Nagasaki and Kazue Yamashita is gratefully acknowledged. Takafumi Oishi, Yoshihiro Koike, Keisuke Naomoto, Yasuko Suzuki are thanked for our teamwork in the field. We thank Ehime University where many thin sections were prepared. We wish to express our gratitude to Tomonori Inada for developing computer programs for data analysis. The paper benefited from the detailed reviews and comments by Tyler MacCready and an anonymous reviewer. Cees W. Passchier is thanked for his editorial corrections of the manuscript.

REFERENCES

Allmendinger, R. W. (1988) Stereonet 4.3a Academic version; a plotting program for orientation data. Computer program.

Baëta, R. D. and Ashbee, K. H. G. (1969a) Slip systems in quartz: I. Experiments. *The American Mineralogist* **54,** 1551–1573.

Baëta, R. D. and Ashbee, K. H. G. (1969b) Slip system in quartz: II. Interpretation. *The American Mineralogist* **54,** 1574–1582.

Banno, S. and Sakai, C. (1989) Geology and metamorphic evolution of the Sanbagawa metamorphic belt, Japan. In *Evolution of Metamorphic Belts*, ed. J. S. Daly, R. A. Cliff and B. W. D. Yardley, **43,** pp. 519–532. Geological Society of London, Special Publication.

Bouchez, J.-L. (1977) Plastic deformation of quartzites at low temperature in an area of natural strain gradient. *Tectonophysics* **39,** 25–50.

Enami, M., Wallis, S. R. and Banno, Y. (1994) Paragenesis of sodic pyroxene-bearing quartz schists: implications for the *P–T* history of the Sanbagawa belt. *Contributions to Mineralogy and Petrology* **116,** 182–198.

Etchecopar, A. (1977) A plane kinematic model of progressive deformation in a polycrystalline aggregate. *Tectonophysics* **39,** 121–139.

Etchecopar, A. and Vasseur, G. (1987) A 3-D kinematic model of fabric development in polycrystalline aggregates: comparisons with experimental and natural examples. *Journal of Structural Geology* **9,** 705–717.

Faure, M. (1983) Eastward ductile shear during the early tectonic phase in the Sanbagawa belt. *The Journal of the Geological Society of Japan* **89,** 319–329.

Fliervoet, T. F. and White, S. H. (1995) Quartz deformation in a very fine grained quartzo-feldspathic mylonite: a lack of evidence for dominant grain boundary sliding deformation. *Journal of Structural Geology* **17,** 1095–1109.

Flinn, D. (1962) On folding during three dimensional progressive deformation. *Geological Society of London* **118,** 385–433.

Ghosh, S. K. (1993) *Structural Geology: Fundamentals and Modern Developments*. Pergamon Press, New York.

Green, H. W., II, Griggs, D. T. and Christie, J. M. (1970) Syntectonic and annealing recrystallization of fine-grained quartz aggregates. In *Experimental and Natural Rock Deformation*, ed. P. Paulitsch, pp. 272–335. Springer.

Guillope, M. and Poirier, J. P. (1979) Dynamic recrystallization during creep of single-crystalline halite: An experimental study. *Journal of Geophysical Research* **84,** 5557–5567.

Hara, I. (1971) An ultimate steady-state pattern of *c*-axis fabric of quartz in metamorphic tectonites. *Geologische Rundschau* **60,** 1142–1173.

Hara, I. and Shiota, T. (1996) Tectonics in the 35km–10km depth of a subduction zone—information from the Sambagawa belt. *Geological Report of the Hiroshima University* **28,** 1–76, in Japanese with English abstract.

Hara, I., Shiota, T., Takeda, K., Okamoto, K. and Hide, K. (1990a) Sambagawa terrane. In *Pre-Cretaceous Terranes of Japan*, eds K. Ichikawa, S. Mizutani, I. Hara, S. Hada and A. Yao, pp. 137–163. Pre-Jurassic Evolution of Eastern Asia, IGCP Project No. 224.

Hara, I., Hide, K., Takeda, K., Tukuda, K., Tokuda, M. and Shiota, T. (1977) Tectonic movement in the Sambagawa belt. In *The Sambagawa belt*, ed. K. Hide, pp. 307–390. Hiroshima University Press, in Japanese with English abstract.

Hara, I., Shiota, T., Hide, K., Okamoto, K., Takeda, K., Hayasaka, Y. and Sakurai, Y. (1990b) Nappe structure of the Sambagawa belt. *Journal of Metamorphic Geology* **8,** 441–456.

Hara, I., Shiota, T., Hide, K., Kanai, K., Goto, M., Seki, S., Kaikiri, K., Takeda, K., Hayasaka, Y., Miyamoto, T., Sakurai, Y. and Ohtomo, Y. (1992) Tectonic evolution of the Sambagawa schists and its implications in convergent margin processes. *Journal of Science of the Hiroshima University Series C* **9,** 495–595.

Heard, H. C. and Carter, N. L. (1968) Experimentally induced "natural" intragranular flow in quartz and quartzite. *American Journal of Science* **266,** 1–42.

Herwegh, M. and Handy, M. R. (1996) The evolution of high-temperature mylonitic microfabrics: evidence from simple shearing of a quartz analogue (norcamphor). *Journal of Structural Geology* **18,** 689–710.

Higashino, T. (1990) The higher grade metamorphic zonation of the Sambagawa metamorphic belt in central Shikoku, Japan. *Journal of Metamorphic Geology* **8,** 413–423.

Hirth, G. and Tullis, J. (1992) Dislocation creep regimes in quartz aggregates. *Journal of Structural Geology* **14,** 145–159.

Isozaki, Y. and Itaya, T. (1990) Chronology of Sanbagawa metamorphism. *Journal of Metamorphic Geology* **8,** 401–411.

Itaya, T. and Takasugi, H. (1988) Muscovite K–Ar ages of the Sanbagawa schists, Japan and argon depletion during cooling and deformation. *Contributions to Mineralogy and Petrology* **100,** 281–290.

Iwasaki, M., Ichikawa, K., Yao, A. and Faure, M. (1984) On the age of Mikabu green rocks, eastern Shikoku, Japan. *Proceedings of the Kansai Branch, Geological Society of Japan* **97,** 21, in Japanese.

Jessell, M. W. (1987) Grain-boundary migration microstructures in a naturally deformed quartzite. *Journal of Structural Geology* **9,** 1007–1014.

Karato, S. and Masuda, T. (1989) Anisotropic grain growth in quartz aggregates under stress and its implication for foliation development. *Geology* **17,** 695–698.

Kojima, J. and Hide, K. (1957) On new occurrence of aegirine augirine augite–amphibole–quartz–schists in the Sambagawa crystalline schists of the Besshi–Shirataki district, with special reference to the preferred orientation of aegirine augite and amphibole. *Journal of Science of the Hiroshima University Series C* **2,** 1–20.

Kojima, J. and Hide, K. (1958) Kinematic interpretation of the quartz fabric of triclinic tectonites from Besshi, Central Shikoku, Japan. *Journal of Science of the Hiroshima University Series C* **2,** 195–226.

Law, R. D. (1986) Relationships between strain and quartz crystallographic fabrics in the Roche Maurice quartzites of Plougastel, western Brittany. *Journal of Structural Geology* **8,** 493–515.

Law, R. D. (1987) Heterogeneous deformation and quartz crystallographic fabric transitions: natural examples from the Moine Thrust zone at the Stack of Glencoul, northern Assynt. *Journal of Structural Geology* **9,** 819–833.

Law, R. D., Casey, M. and Knipe, R. J. (1986) Kinematic and tectonic significance of microstructures and crystallographic fabrics within quartz mylonites from the Assynt and Eriboll regions of the Moine thrust zone, NW Scotland. *Transactions of the Royal Society of Edinburgh: Earth Sciences* **77,** 99–125.

Law, R. D., Knipe, R. J. and Dayan, H. (1984) Strain path partitioning within thrust sheets: microstructural and petrofabric evidence from the Moine Thrust zone at Loch Eriboll, northwest Scotland. *Journal of Structural Geology* **6,** 477–497.

Lisle, R. J. (1985) The use of the orientation tensor for the description and statistical testing of fabrics. *Journal of Structural Geology* **7,** 115–117.

Lister, G. S. and Dornsiepen, U. F. (1982) Fabric transitions in the Saxony granulite terrain. *Journal of Structural Geology* **4,** 81–92.

Lister, G. S. and Hobbs, B. E. (1980) The simulation of fabric development during plastic deformation and its application to quartzite: the influence of deformation history. *Journal of Structural Geology* **2,** 355–370.

Lister, G. S., Paterson, M. S. and Hobbs, B. E. (1978) The simulation of fabric development in plastic deformation and its application to quartzite: The model. *Tectonophysics* **45,** 107–158.

Lloyd, G. E. and Freeman, B. (1991) SEM electron channelling analysis of dynamic recrystallization in a quartz grain. *Journal of Structural Geology* **13,** 945–953.

Lloyd, G. E. and Freeman, B. (1994) Dynamic recrystallization of quartz under greenschist conditions. *Journal of Structural Geology* **16,** 867–881.

Marjoribanks, R. W. (1976) The relation between microfabric and strain in a progressively deformed quartzite sequence from central Australia. *Tectonophysics* **32,** 269–293.

Masuda, T. (1982) A microstructural sequence of quartz schists in central Shikoku, Southwest Japan. *Tectonophysics* **83,** 329–345.

Masuda, T. and Fujimura, A. (1981) Microstructural development of fine-grained quartz aggregates by syntectonic recrystallization. *Tectonophysics* **72,** 105–128.

Miller, D. M. and Christie, J. M. (1981) Comparison of quartz microfabric with strain in recrystallized quartzite. *Journal of Structural Geology* **3,** 129–141.

Miyashiro, A. (1961) Evolution of metamorphic belts. *Journal of Petrology* **2,** 277–311.

Nadai, A. (1963) *Theory of Flow and Fracture of Solids*. McGraw-Hill, New York.

Oyagi, N. (1964) Structural analysis of the Sambagawa crystalline schists of the Sazare mining district, central Shikoku. *Journal of Science Hiroshima University Series C* **4,** 271–332.

Price, G. P. (1985) Preferred orientations in quartzites. In *Preferred Orientation in Deformed Metals and Rocks: An Introduction to Modern Texture Analysis*, ed. H.-R. Wenk, pp. 385–406. Academic Press.

Sakakibara, N., Hara, I., Kanai, K., Kaikiri, K., Shiota, T., Hide, K. and Paulitsch, P. (1992) Quartz microtextures of the Sambagawa schists and their implications in convergent margin processes. *The Island Arc* **1,** 186–197.

Schmid, S. M. and Casey, M. (1986) Complete fabric analysis of some commonly observed quartz *c*-axis patterns. In *Mineral and Rock Deformation: Laboratory studies—The Paterson volume*, eds B. E. Hobbs and H. C. Heard, pp. 263–286. Geophysical Monograph. **36**.

Shimizu, I. (1988) Ductile deformation in the low-grade part of the Sambagawa metamorphic belt in the northern Kanto mountains, central Japan. *The Journal of the Geological Society of Japan* **94,** 609–628, in Japanese with English abstract.

Tagami, M. (1998) *c*-axis fabrics and microstructures in quartz schist from the Sambagawa metamorphic belt, central Shikoku, Japan. Unpublished Ph.D. thesis. Hiroshima University, Japan.

Takeshita, T. (1996) Estimate of the physical conditions for deformation based on *c*-axis fabric transitions in naturally deformed quartzite. *The Journal of the Geological Society of Japan* **102,** 211–222, in Japanese with English abstract.

Takeshita, T. and Wenk, H.-R. (1988) Plastic anisotropy and geometrical hardening in quartzites. *Tectonophysics* **149,** 345–361.

Toriumi, M. (1982) Strain, stress and uplift. *Tectonics* **1,** 57–72.

Trépied, L. and Doukhan, J.-C. (1982) Evidence of $<a + c>$ dislocations in synthetic quartz single crystals compressed along *c* axis. *Bulletin de Minéralogie* **105,** 176–180.

Tullis, J. (1977) Preferred orientation of quartz produced by slip during plane strain. *Tectonophysics* **39,** 87–102.

Tullis, J., Christie, J. M. and Griggs, D. T. (1973) Microstructures and preferred orientations of experimentally deformed quartzites. *Geological Society of America Bulletin* **84,** 297–314.

Wallis, S. R., Banno, S. and Radvanec, M. (1992) Kinematics, structure and relationship to metamorphism of the east west flow in the Sanbagawa Belt, southwest Japan. *The Island Arc* **1,** 176–185.

Wenk, H.-R., Canova, G., Molinari, A. and Kocks, U. F. (1989) Viscoplastic modeling of texture development in quartzite. *Journal of Geophysical Research* **94,** 17,895–17,906.

Woodcock, N. H. (1977) Specification of fabric shapes using an eigenvalue method. *Geological Society of America Bulletin* **88,** 1231–1236.